ACS APPLIED MATERIALS & INTERFACES

www.acsami.org

Research Article

Differentiation of Multiple Mechanical Stimuli by a Flexible Sensor Using a Dual-Interdigital-Electrode Layout for Bodily Kinesthetic Identification

Xin Li,[▽] Jinwei Cao,[▽] Huayang Li,[▽] Pengtao Yu, Youjun Fan, Yuchuan Xiao, Yiming Yin, Xuejiao Zhao, Zhong Lin Wang,* and Guang Zhu*

Cite This: https://doi.org/10.1021/acsami.1c05572

Read Online

ACCESS | Metrics & More | Article Recommendations | Supporting Information

ABSTRACT: Human bodily kinesthetic sensing is generally complicated and ever-changing due to the diversity of body deformation as well as the complexity of mechanical stimulus, which is different from the unidirectional mechanical motion. So, there exists a huge challenge for current flexible sensors to accurately differentiate and identify what kind of external mechanical stimulus is exerted via analyzing digital signals. Here, we report a flexible dual-interdigital-electrode sensor (FDES) that consists of two interdigital electrodes and a highly pressure-sensitive porous conductive sponge. The FDES can precisely identify multiple mechanical stimuli, e.g., pressing, positive bending, negative bending, *X*-direction stretching, and *Y*-direction stretching, and convert them into corresponding current variation signals. Moreover, the FDES exhibits other exceptional properties, such as high sensitivity, stretchability, large measurement range, and outstanding stability, accompanied by simple structural design and low-cost processing simultaneously. Additionally, our FDES successfully identifies various complex activities of the human body, which lays a foundation for the further development of multimode flexible sensors.

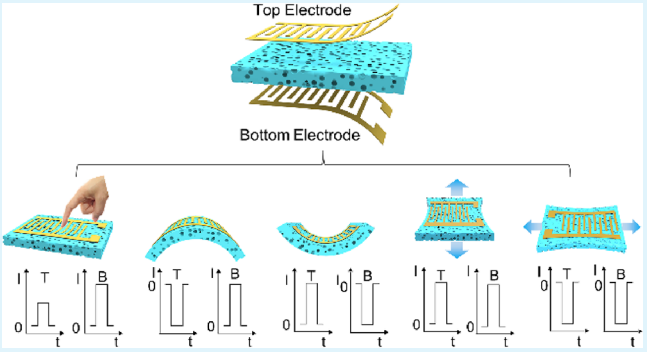

KEYWORDS: *flexible sensors, multiple mechanical stimuli, interdigital electrodes, resistance effect, bodily kinesthetic identification*

1. INTRODUCTION

Flexible and stretchable sensing devices have consistently been applied in the accurate visualization of physiological signals and mechanical deformations, attracting increasing attention to flexible electronics,[1,2] human−robotic interfaces,[3,4] biomedical devices, etc.[5,6] Flexible sensors, the basic functional units in sensing devices, are of profound importance in effective body motion monitoring.[7−12] Recently, a series of mechanical sensors (for pressure, strain, or bending) with an outstanding flexibility, high gauge factor, and broad sensing range were perspicuously presented.[13−17] Lee et al. developed a flexible sensor with high sensitivity and linear response over an exceptionally broad pressure range based on a ferroelectric composite material and a multilayer interlocked microdome geometry.[16] Liu et al. reported an all-textile pressure sensor that had excellent sensitivity due to the combination of Ni coatings and CNT fabrics.[18] However, a single sensing capability cannot accurately detect multiple mechanical stimuli simultaneously.[19,20] There are still major challenges for flexible sensors that possess complex-deformation-sensing capabilities.

Some researchers proceed to develop flexible sensors that can respond to multiple mechanical stimuli simultaneously, like pressure, strain, bending, etc.[21−23] Unfortunately, most of these multimode flexible sensors can solely convert different mechanical stimuli into the same tendency of resistance change, failing to differentiate the types of stimuli.[24−27] We summarized the research progress of sensors based on multiple mechanical stimuli in recent years, as shown in Table S1.[28−33] Especially, Pang et al.[30] reported a multimodal flexible sensor based on 1D conductive fibers that failed to detect the deformation in a 2D plane. Bao et al.[28] used three independent variants to differentiate multiple mechanical stimuli, but they worked poorly at small deformations due to the insensitivity of the plane electrodes. Therefore, the signal analysis system cannot precisely decouple and identify the complex multi-dimensional mechanical stimuli according to electrical resistance-varying signals. As a result, a huge challenge remains

Received: March 25, 2021
Accepted: May 13, 2021

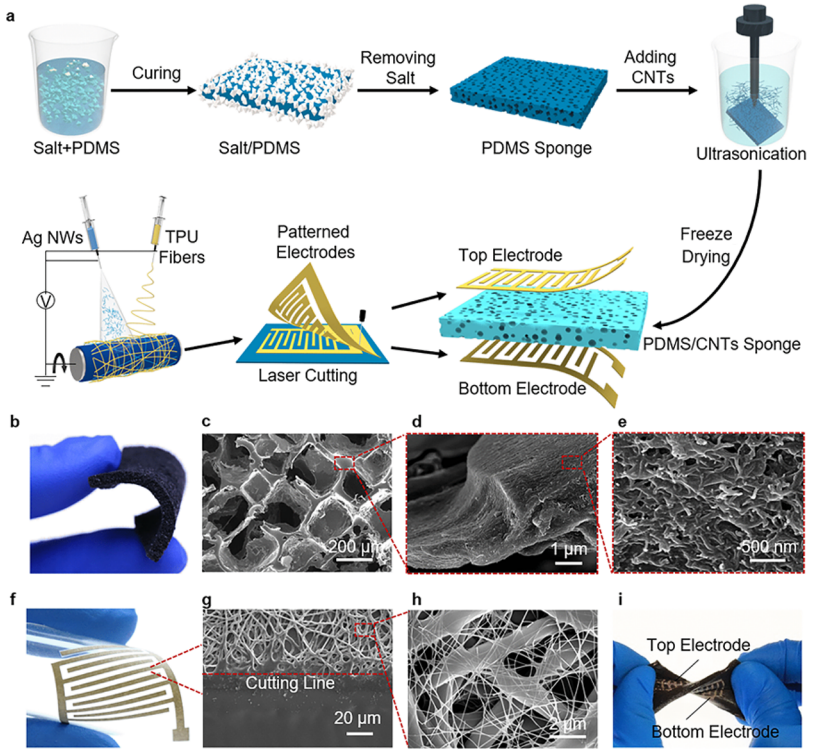

Figure 1. Dual-interdigital-electrode flexible sensor. (a) Fabrication process and structure of the FDES with two interdigital electrodes. (b) Digital photograph of the fabricated CNTs/PDMS sponge. (c–e) Representative SEM images of the CNTs/PDMS sponge with different magnifications. (f) Optical image showing the bendability of the interdigital electrode. (g) SEM image of the line boundary in the pattern. (h) Details of the stretchable nanonetwork electrode. (i) Photograph showing the flexible sensor at 180° twisted states.

for the flexible sensors that can simultaneously differentiate and identify multiple external stimuli, including pressure, bending and strain, etc. In addition, other practical issues such as flexibility, stretchability, and durability also need to be properly addressed so as to satisfy higher application and commercial demands.

In this study, we report a flexible dual-interdigital-electrode sensor (FDES) that possesses the capabilities for precisely differentiating multiple mechanical stimuli based on the different current variation signals using an unprecedented dual-interdigital-electrode layout. The FDES is composed of a carbon nanotubes/polydimethylsiloxane (CNTs/PDMS) porous sponge sandwiched by two sets of interdigital electrodes. The conductive porous sponge guarantees excellent performance of the sensor (high sensitivity, large measurement range, and high stability) owing to its high specific surface conductive area, outstanding mechanical flexibilities, and compressibility.[28,34−36] More specifically, when the FDES is subjected to external stimulation (such as pressure, stretching, and bending), the top and bottom interdigital electrodes made responses to the applied force and converted them into current variation signals, respectively. Whereafter, the response current direction and magnitude of the two electrodes work together to reversely speculate the type of external stimulus and the degree of deformation. Furthermore, the flexible sensing device exhibits high sensitivity, stretchability, large measurement range, and outstanding stability, accompanied by cost-effective operation. These distinctive performances have further been proven through bodily kinesthetic identification application, confirming its promising utility for a new generation of accurately identifying the complexity of human body motions.

2. RESULTS AND DISCUSSION

Figure 1a illustrates the fabrication process of the FDES, which consists of a conductive sponge active layer and two interdigital electrodes. More specifically, the active layer was constructed by the deposition of CNTs on an elastic PDMS sponge. To fabricate this conductive porous sponge, a sacrificial template method was applied, as shown in Figure 1a. The sodium chloride (NaCl) particles were added into uncured PDMS liquid, which was followed by uniform mixing and thermal curing, and then the NaCl particles were washed away by soaking this layer in deionized water. After that, the PDMS sponge was immersed in the dispersion of CNTs and a cross-linking agent (chitosan) with an ultrasonic treatment in a low temperature. Subsequently, the stretchable conductive PDMS sponge filled with CNTs was fabricated after vacuum freeze-drying.[37,38] Above and below the conductive active layer, there are two nanonetwork skin interdigital electrodes, which were fabricated based on the protocol reported recently.[39−41] According to the technology of electrospray and electrospinning, silver nanowires and polyurethane nanofibers were simultaneously collected on a metal collector layer by layer to form a conductive film, as portrayed in Figure 1a. After the laser scribing on the conductive film with the designed patterns, the interdigital electrodes were obtained. Finally, the electrodes were transferred on 3M VHB adhesive tapes and then the tapes, working as an encapsulation layer, were used to fix the electrodes on the top and bottom of the conductive sponge. It is worthwhile to note that all the fabrication process is green, low cost, simple, and easily scalable, which makes the FDES promising for a large amount of practical applications. Additionally, the fabrication details are further described in Section 4. Figure 1b describes the

https://doi.org/10.1021/acsami.1c05572
ACS Appl. Mater. Interfaces XXXX, XXX, XXX−XXX

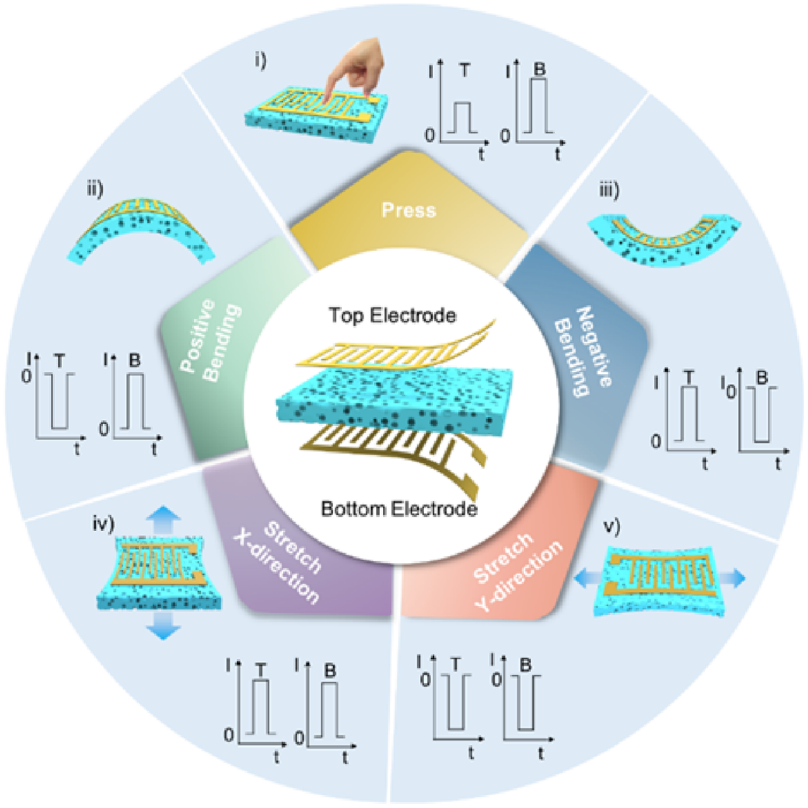

Figure 2. Schematic illustration of the sensing mechanism and current changes in response to the recorded various physiological signals.

flexibility and bendability of the conductive CNTs/PDMS sponge with open networks of pores. To zoom in, a scanning electron microscopy (SEM) image of the conductive sponge is shown in Figure 1c, indicating that the microstructure of the sponge is the inverse matrix of the NaCl particles with an average pore size of 200 μm. A magnified view of the inner surface clearly shows that the CNTs are conformally attached to the walls of elastic porous sponge PDMS scaffolds (Figure 1d) to form conductive pathways (Figure 1e). The electrical and mechanical properties of the conductive porous sponge are adjusted and controlled by PDMS scaffolds as well as CNT contents, respectively. Therefore, there is an indistinguishable difference between the sponges with CNTs (1.3%) and without CNTs in terms of the tensile strength (Figure S1a, Supporting Information) but a noticeable difference for conductivity (shown in Figure S1b, Supporting Information). This novel design not only leads to excellent break elongation (120%) but also accounts for high sensitivity for the exertion of multiple physiological motions, making the sensor practically reliable and durable. Next, as for the interdigital electrodes, laser cutting was utilized to fabricate high-precision electrodes without any mask. A piece of the prepared interdigital electrode with clear-cutting lines is exhibited in Figure 1f. At higher magnification, the accuracy of the cutting line is clear (as shown in Figure 1g). Figure 1h is down to the finest detail of the stretchable nanonetwork electrode, in which the silver nanowires are evenly interspersed in polyurethane nanofiber networks to form conductive pathways. Figure 1i shows the optical image of a representative flexible dual-interdigital-electrode sensor when twisted at 180°, revealing excellent flexibility as well as mechanical robustness.

The FDES operated on the highly sensitive resistance effect of the conductive CNTs/PDMS porous active layer sandwiched between two interdigital electrodes. When any mechanical stimuli occur on the FDES, the top and bottom interdigital electrodes go through different movement trends. Therefore, the response trends and magnitudes of the two electrodes work together to reversely speculate and pinpoint what kinds of external stimuli were exerted and the degree of deformation. Figure 2 discloses the working principle of the FDES in terms of its response to the mechanical changes. The FDES can successfully differentiate and identify various mechanical stimuli, including pressing, positive bending, negative bending, and *X*-direction and *Y*-direction stretching. In addition, there is a one-to-one correspondence between each kind of deformation and the resistive variation trend. The response of the sensor to different deformations would be respectively explained in the subsequent section.

Compression always comes to the first remarkable deformation of the sensing device. Figure 3a demonstrates the specific deformation of the FDES when pressed by a finger or a nonplanar surface. Applying an external pressure would cause an increase in the contact area between the CNTs/PDMS sponge and two interdigital electrodes, which can generate more conductive pathways between them. However, for the top interdigital electrode, finger electrode length (d) and insulating gap width (b) increased with the enhancement of pressure, which will lead to an increase in resistance. The detailed size of the interdigital electrode is depicted in Figure S2 (Supporting Information). Allowing for the double action of pressure and deformation on the top interdigital electrode, the bottom interdigital electrode shows larger changes in current than the top interdigital electrode when the same pressure is applied. To explore the pressure-sensing properties, the current responses were measured when applying different forces on the device. The sensing device was fixed on a

https://doi.org/10.1021/acsami.1c05572
ACS Appl. Mater. Interfaces XXXX, XXX, XXX−XXX

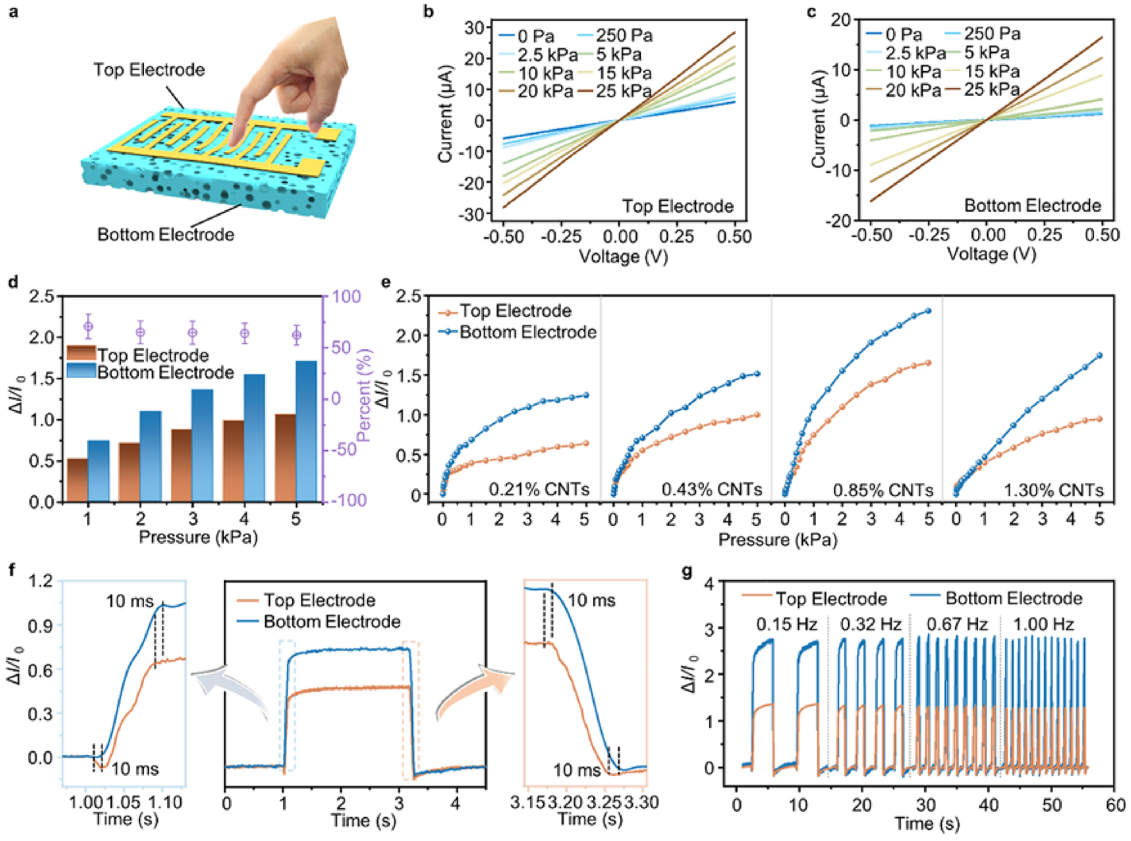

Figure 3. Evaluation of pressure-sensing performances. (a) Schematic illustration of the direction of the applied pressure and the relative position of the double electrodes. (b, c) *I*−*V* curves of the top and bottom electrodes in the FDES, respectively. (d) Difference in current changes between the top and bottom electrodes under different pressures. (e) Pressure response curves of double electrodes of the FDES for different ratios of CNTs/PDMS (0.21−1.30 wt %). (f) Delay of response (left)/release (right) time of the bottom electrode with loading/unloading pressure. (g) Relative current variation under cyclic loading/unloading at different frequencies.

homemade system (Figure S3, Supporting Information), which detects the current change of the two interdigital electrodes simultaneously. The FDES showed a steady response to each static pressure (Figure 3b,c), indicating that the resistances (slope of *I*−*V* curves) remained constant. At the same time, the slope of the *I*−*V* curves increased obviously when the applied pressure changes from 0 to 25 kPa. In addition, the sensitivity of the sensing device is generally defined as $S = (\Delta I/I_0)/\Delta P$, where ΔI is the relative current change, I_0 is the current without any applied pressure, and ΔP is the change of the applied pressure. According to the experimental results, the FDES based on porous sensing layers and nanonetwork interdigital electrodes showed high sensitivity. As shown in Figure S4 (Supporting Information), in a low-pressure region under 1 kPa, the sensitivity of the top electrode is 0.75 kPa^{-1} and that of the bottom electrode is 1.1 kPa^{-1}. In the high-pressure regions over 1 kPa, the sensitivity of the top electrode is 0.23 kPa^{-1} and that of the bottom electrode is 0.3 kPa^{-1}. Moreover, the bottom electrode has higher sensitivity compared to the top electrode at the same sensing device, which is a characteristic rule when the FDES is pressed. Deserved to be mentioned, the difference in current changes between the top and bottom electrodes was slowly increased with the increase in compressive load (Figure 3d). Figure 3e shows the relative current change of the sensors with various CNT ratios in the conductive sponges when the applied pressure increased from 0 to 5 kPa. It was found that the sensors with a CNT ratio of 0.85% have the highest sensitivity compared to the others (0.21, 0.43, and 1.30%). This is because, within a certain range, more carbon nanotubes will form more conductive pathways when pressed. However, the excess addition of CNTs will significantly increase conductivity (when the ratio of CNTs is more than 1.30%), in return affecting its further increase in corresponding conductive pathways. In the following experiments, it is observed that the delay response of the bottom electrode is 10 ms longer than that of the top electrode due to the excellent elasticity of the sponge when the sensor responded to a pressure of 1.5 kPa (Figure 3f). This is another important characteristic rule when the FDES is pressed. As shown in Figure 3g, the relative resistance changes of the FDES exhibit almost no frequency dependence within the tested frequency range from 0.15 to 1.00 Hz in the top and bottom electrodes. In addition, the cycling stability of the flexible sensing device was measured under a pressure of 5 kPa. As shown in Figure S5 (Supporting Information), our FDES represented excellent reproducibility and durability with negligible signal variations in 8000 loading and unloading tests.

Next, the second major deformation of the FDES is bending. The bending and initial state of the as-prepared flexible sensor are schematically illustrated in Figure 4a. Here, the initial length of the sensor was termed as d_0 and the moving distance in the bending state was Δd. The bending angle θ was defined as the external angle of the two ends, as shown in Figure 4a. Figure 4b shows a positive bending flexible sensor, in which the top electrode is on the outer arc with the maximum

https://doi.org/10.1021/acsami.1c05572
ACS Appl. Mater. Interfaces XXXX, XXX, XXX−XXX

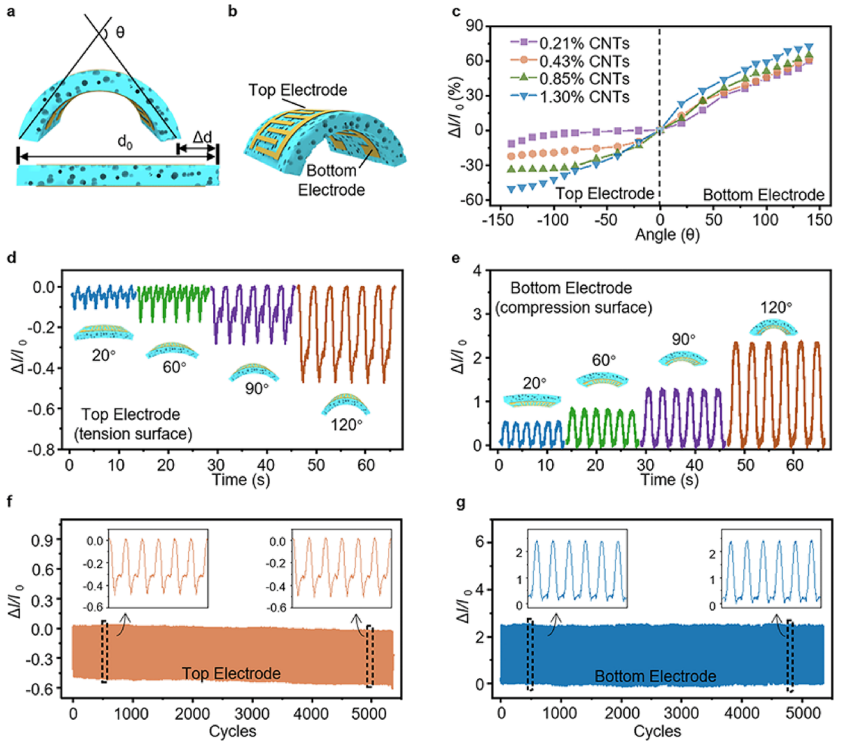

Figure 4. Sensing performance of the FDES under bending states. (a) Schematic illustration of the bending FDES. (b) Defining the relative positions of the top and bottom electrodes. (c) Relationship between relative current changes and bending angles for different ratios of CNTs/PDMS. (d) Relative current changes of the top electrode and (e) bottom electrode when bending the FDES at different angles (20, 60, 90, and 120°), respectively. (f, g) Bending responses of the FDES over 5000 cyclic tests.

tension. Meanwhile, the negative bending, in contrast, is another bending deformation with the top electrode located on the inner arc under the largest compression. It is worth noting that in order to avoid the pressure of the packaging layer on the upper electrode during the bending process, packaging materials with low Young's moduli are necessary. This experiment adopts polyurethane nanofibers combined with VHB as the low Young's modulus packaging layer (Figure S6, Supporting Information). The TPU nanofiber has better tensile properties (600%) and lower Young's modulus compared to a commercial TPU film. Because the two kinds of bending are completely opposite and extremely symmetric, only the positive bending was discussed in detail. Figure 4c shows the relative current change of the sensors with different CNT contents when the bending angle θ increased from 0 to 150°. Additionally, the current of the top electrode (on the tensile surface) gradually decreased with the increase in the bending angle due to the coupling of conductive sponge deformation and increasing insulating gap width (b), while the current of the bottom electrode (on the compressive surface) gradually increased with the increase in bending angle, and this is because of the decreased b and compression of the conductive sponge. It was found that a CNT ratio of 1.30% has the highest sensitivity compared to the other ratios (0.21, 0.43, and 0.85%). As shown in Figure 4d,e, under various dynamic bending (20, 60, 90, and 120°), the FDES revealed stable and repeatable responses. Moreover, reliability and stability are also common aspects of concern for evaluating sensors. The sensor showed a long-term reliable operation for up to 5300 cycles under a bending angle of 120° (Figure 4f,g). Additionally, the insets show that the amplitude of the current change hardly varied after the repeated tests.

The third inherent mode of the FDES is the perception of stretching. Figure 5a shows the diagram of the shape and size of the interdigital electrode before strain. The resistance of the interdigital electrode in a single period is divided into two small rectangular resistors, R_1 and R_2, as shown in Figure 5b. A more detailed analysis of the particular expression of R is thoroughly presented in the Supporting Information. The resistance of the interdigital electrode R is equivalent to nine R_1 in parallel. Based on the final equation of R (eq 5 in the Supporting Information), the value of R dominantly depends on the value of b, d, and square resistance of the sensing layer, which has been proven in the Supporting Information. When the stress was applied in the X-direction, the current of the electrode gradually increased with the stretch due to the coupling of conductive sponge deformation as well as the decrease in insulating gap width (Figure 5b). On the contrary, if the stress was applied in the Y-direction, then the current of the electrode would gradually decrease (Figure 5b). Upon X-direction and Y-direction stretching, the resistance of the interdigital electrode would decrease and increase, respectively. Figure 5c,d shows the two directions (X-direction and Y-direction) of the stresses that were being applied on the FDES, respectively. Here, the X-direction is parallel to the fingers of the interdigital electrode and the Y-direction is perpendicular to them. Due to the symmetry of this sensor, the two electrodes exhibit a high consistency in terms of the variation trend and magnitude of their resistance when the sensor is stretched. Therefore, one of the pattern electrodes was studied in the subsequent stretch test. It is seen from Figure 5c,d that a different resistance−strain relationship was obtained after the stress was applied in the X- and Y-directions, respectively. This was due to the anisotropic geometry of the electrode design.

https://doi.org/10.1021/acsami.1c05572
ACS Appl. Mater. Interfaces XXXX, XXX, XXX−XXX

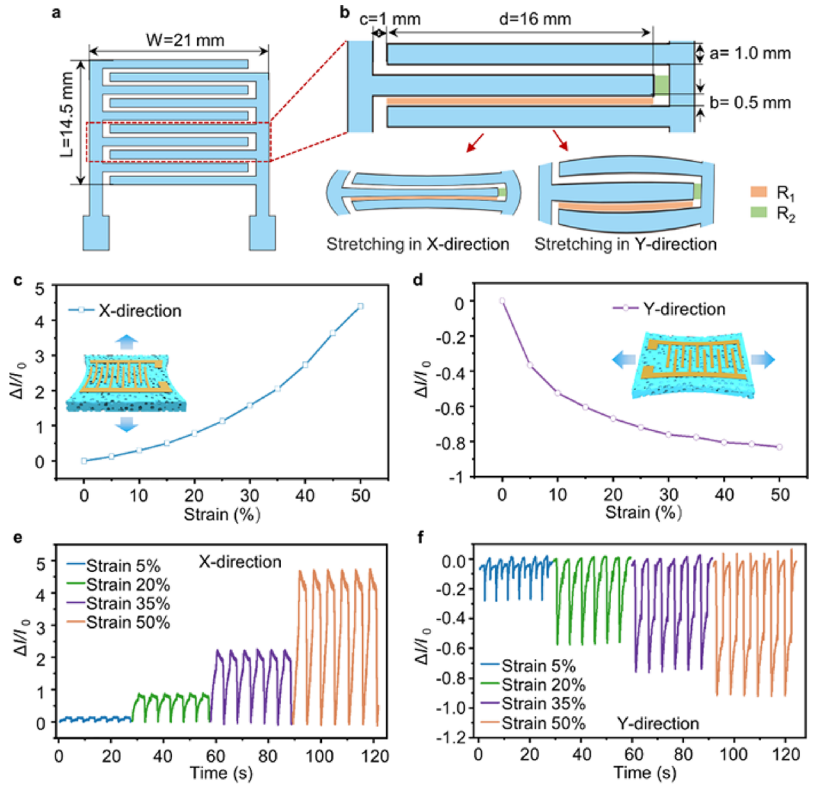

Figure 5. Strain performance of the FDES. (a) Diagram of the shape and size of the interdigital electrode before strain. (b) Corresponding physical models under different deformation conditions, including deformation in *X*- and *Y*-directions. (c) Relative current changes of the FDES versus the applied strain in the *X*-direction and schematic illustration of the strain direction. (d) Relative current changes of the FDES versus the applied strain in the *Y*-direction and schematic illustration of the strain direction. Relative current changes at different strains (5, 20, 35, and 50%) in the (e) *X*-direction and (f) *Y*-direction, respectively.

The inset of Figure 5c,d shows the deformation of the FDES in detail. In addition, the current responses to applied strains with different degrees and different directions are clearly measured and depicted in Figure 5e,f. Its stable and reliable response paves the way for applications in motion detection. We have also explored the signal stability over 2000 stretching−releasing cycles (Figure S7a,b, Supporting Information). The initial and final cycles cause no obvious difference in the resistance change amplitude, which indicates the excellent durability of the flexible sensor.

The working pattern of bodily kinesthesia and mechanical stimulus is always the random superposition of various actions such as pressing, bending, and stretching. In a basketball game, for example, the fingers bend and suffer from pressure during shooting. Figure 6a illustrates a silhouette of two basketball players who present various body movements for different purposes in a game, such as offense, cutting, passing, and shooting. Also, it is a superimposed effect that induces the change trend of electric current under complicated bodily kinesthesia. Over here, the FDES based on two interdigital electrodes demonstrates a great advantage in the simple deformation (such as pressure, stretching, and bending) and complex body motion detection. In the subsequent figure (Figure 6b), we presented two explanatory formulas to clearly illustrate the electric current variation trend responding to complex stimulus. To further verify these formulas, a series of application scenarios are designed where the FDES demonstrated excellent sensing capabilities in accurate bodily kinesthetic identification (Figure 6c−g). The FDES was attached to the knuckles of fingers, as shown in Figure 6c−e, to detect and identify the finger movements during clicking the mouse, bending, and picking up the beaker, which was also demonstrated in Video S1 (Supporting Information). When the finger left clicks, two interdigital electrodes were under pressure from the finger and presented a consistent current change due to the similar deformations of electrodes (Figure 6c). In bending, however, the top and bottom interdigital electrodes show different movements: the top electrode suffered more deformation and presented more changes in current (Figure 6d). In the scenario of picking up a beaker, the fingers first bent upward and then pressed the beaker, which consequently led to two peaks (bending and pressure peaks) in current monitoring signals (Figure 6e). This current variation trend is fully coherent to the formulation in Figure 6b(i). Notably, during the stage of putting down the beaker, the finger recovered from two kinds of deformations to an initial state simultaneously, so there was only one peak corresponding to the release stage. Furthermore, Figure 6f,g shows the optical images and corresponding current signal of the FDES to identify the motion of the wrist. When the wrist is moving, the two electrodes were stimulated by the same deformations (stretch or compression) due to the influence of a neutral surface. Far away from the neutral surface, the top electrode presented greater relative current variation than the bottom electrode despite folding backward (Figure 6f) or forward (Figure 6g), which can be seen in Video S2 in the Supporting Information. Figure 6h shows the optical image and relative current signal changes responding to elbow bending. When the elbow bends, the electrodes produce a single bending signal. If the elbow encounters external stimuli during bending, as

https://doi.org/10.1021/acsami.1c05572
ACS Appl. Mater. Interfaces XXXX, XXX, XXX−XXX

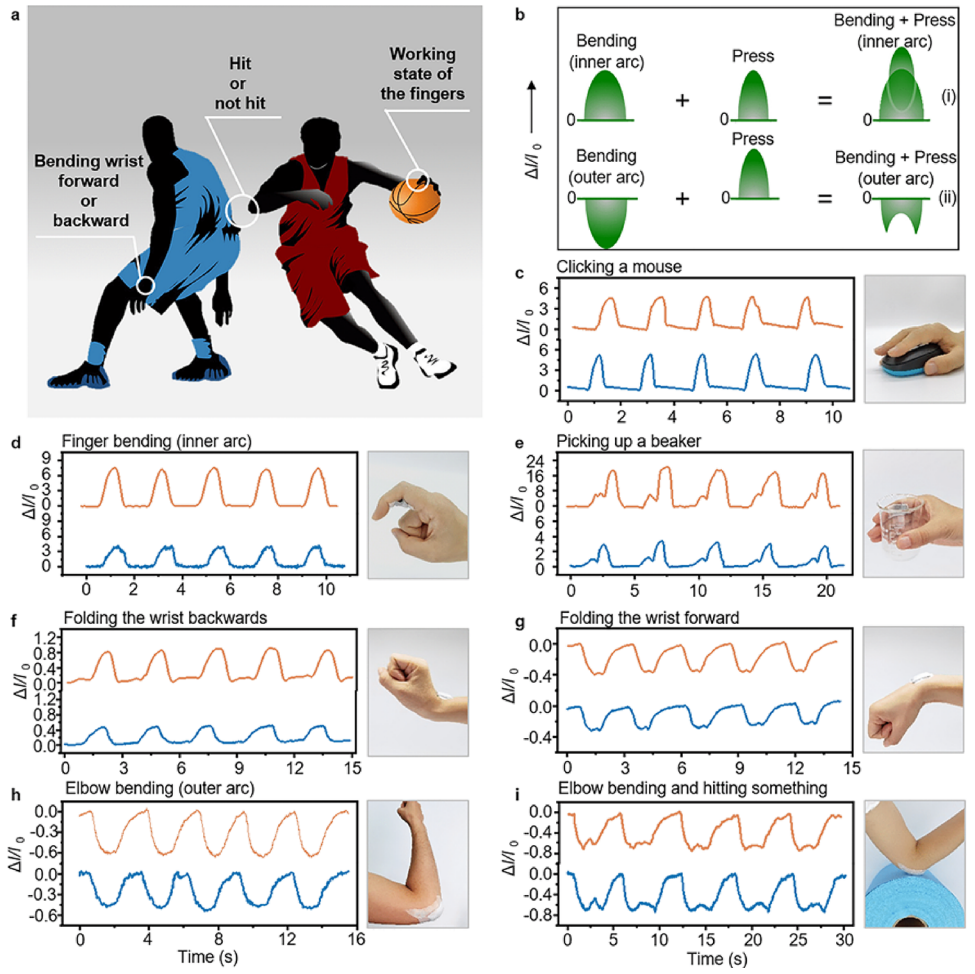

Figure 6. Applications of the FDES in accurate bodily kinesthetic identification. (a) Schematic illustration of the diversity and complexity of human deformation during movement. (b) Superposition principle of current corresponding to complex deformation. (c–e) Optical images and current signal responding to various finger motions: (c) clicking a mouse, (d) bending, and (e) picking up a beaker. (f, g) Optical images and corresponding current signal of the FDES to identify the motion of the wrist: (f) folding the wrist backward and (g) folding the wrist forward. (h) Optical image and current signal responding to elbow bending. (i) Optical image and corresponding current signal of elbow bending and hitting something.

shown in Figure 6i, then there is an additional signal in the primary bending signal to express the presence of external stimuli. This current variation trend is fully consistent with the formula in Figure 6b(ii). Movement monitoring of the elbow can be seen in Video S3 in the Supporting Information. Therefore, our FDES shows a unique ability in multiple movements' identification.

3. CONCLUSIONS

In order to improve the ability of the flexible sensor to accurately identify multiple deformations and external stimuli, we have developed a dual-interdigital-electrode flexible sensor that consists of two interdigital electrodes and a highly pressure-sensitive porous sponge. This unique mechanism makes our FDES successfully differentiate various mechanical stimuli, i.e., pressing, bending, and *X*-direction and *Y*-direction stretching, and realize a one-to-one correspondence between each kind of deformation and the current variation trend. Notably, our sensing device exhibited high sensitivity, stretchability, large measurement range, and outstanding stability simultaneously. All of these, consequently, enable this FDES to successfully identify various complex activities of the human body and lay a foundation for the further development of flexible sensors.

4. EXPERIMENTAL SECTION

4.1. Fabrication Process of the FDES. The FDES, a symmetrical multilayered structure, consists of a highly pressure-sensitive CNTs/PDMS porous sponge, two interdigital electrodes, and necessary encapsulation layers. The fabrication process of the FDES is as follows:

4.1.1. Fabrication Process of the CNTs/PDMS Porous Sponge. First, 10 g of PDMS prepolymer and 1 g of curing agent (10:1) were added into a beaker and mixed thoroughly before use. Then, 100 g of NaCl (sodium chloride, Aladdin) particles as sacrifice templates was added in the beaker and kept under stirring for 1 h. Then, the mixture was transferred into a cubic mold (40 × 40 × 3 mm) and compacted under pressure. Next, the mold was placed in an oven at 75 °C for 2 h to make PDMS completely cured. Subsequently, this cured composite body was removed from the mold and after the NaCl particles were cleaned up by ultrasonication (80 W, 2 days) in deionized (DI) water, the PDMS porous sponge was obtained. The CNTs can be uniformly dispersed in water to get a CNT dispersion at different concentrations with an ultrasonic method. Then, 49.5 mL of DI water, 0.5 mL of acetic acid, and 0.25 g of chitosan (Aladdin) were added in a 100 mL beaker to get a 0.5% chitosan solution as a physical cross-linking agent after stirring for 30 min. In the next step, the PDMS porous sponge

https://doi.org/10.1021/acsami.1c05572
ACS Appl. Mater. Interfaces XXXX, XXX, XXX−XXX

was put into the CNT dispersion with ultrasonic treatment for 30 min, which makes the holes of the PDMS sponge filled with CNT dispersion. Then, 2 mL of 0.5% chitosan solution was added to cross-linking CNTs after ultrasonic treatment for 10 min. Finally, the CNTs/PDMS porous sponge was prepared from the composite of the PDMS porous sponge and CNT dispersion through vacuum freeze-drying.

4.1.2. Fabrication Process of the Interdigital Electrode. The main process was divided into two sections, i.e., preparation of nanonetwork skin electrodes and patterning. First, skin electrodes were fabricated by the techniques of electrospray and electrospinning reported recently. Polyurethane masterbatches (TPU, Elastollan, 1180 A) were added to the solvent hexafluoroisopropanol (HFIP, Aladdin) and then stirred at room temperature for 6 h to get a 4 wt % TPU solution. Silver nanowires as conductive fillers were evenly dispersed in alcohol at a concentration of 1.5 mg/mL. Electrospinning TPU nanofibers and electrospraying silver nanofibers were simultaneously carried out on an electrospinning device (Ucalery, ET-2535H). During the spinning process, the pump rates of TPU electrospinning and silver nanofiber electrospraying were set at 0.04 and 0.4 mL min^{-1}, respectively. The positive voltage of electrospinning and spraying was 15 kV, and the negative voltage was 2 kV. The nanonetwork electrode that consisted of silver nanofibers and TPU nanofibers was collected on a metal collector of a winding roller. The nanonetwork electrode was peeled off the metal collector with the help of a polyethylene terephthalate (PET) frame, and then the electrode was attached close to a polydimethylsiloxane (PDMS) film in a wetted state. Then, the nanonetwork electrode was cut into interdigital with designed patterns using a commercial laser cutter.

4.1.3. Preparation of the FDES. A TPU nanofiber film was prepared by the electrospinning method, and then the TPU film was peeled off the metal collector with the help of a polyethylene terephthalate (PET) frame. One side of VHB tape was pasted onto the TPU nanofiber film, whereas the other side bonded with the prepared interdigital electrode. Conductive wires were glued with silver paste at the two ends of the interdigital electrode. Finally, parts of VHB tape were exposed and fixed to the conductive sponge through the gaps inside the patented interdigital electrode, which contributes to our multistimuli-differentiable sensor.

4.2. Performance Tests and Characterization of the FDES. A computer-controlled stepper motor (Linmot E1100) with a hemispherical surface was used to provide external pressure, and the value of the external pressure was measured using a digital force gauge (Mark-10 Corporation, M5-20). The bending and stretching deformations of the device were precisely controlled by the stepper motor. Two independent digital source meters (Keithley 2611B/E) were utilized to measure the $I-t$ curve of the two interdigital electrodes in real time, respectively, and the source−drain voltage was set at 0.1 VDC. An electrochemical workstation (CH Instruments, CHI660E) was used to measure the $I-V$ curve under different external pressures. The microstructures of the CNTs/PDMS porous sponge as well as the nanonetwork electrode were characterized using a Nova NanoSEM 450 (FEI). A universal testing machine was used to test the tensile properties of each layer of the FDES.

■ ASSOCIATED CONTENT

Supporting Information

The Supporting Information is available free of charge at https://pubs.acs.org/doi/10.1021/acsami.1c05572.

Resistance derivation of the interdigital electrodes, research progress of sensors based on multiple mechanical stimuli, properties of the CNTs/PDMS sponge, detailed size of the interdigitated electrode, homemade two sets of an interdigitated electrode test system, sensitivity of our FDES, reliability test of the FDES under repeated loading and unloading, comparison between TPU nanofibers and commercial TPU films, physical models under strain conditions, and stability analysis under strain conditions (PDF)

Video of three typical finger movements (AVI)

Video of the bending of the wrist (AVI)

Video of the movement recognition of the elbow (AVI)

■ AUTHOR INFORMATION

Corresponding Authors

Zhong Lin Wang − *CAS Center for Excellence in Nanoscience, Beijing Key Laboratory of Micro-Nano Energy and Sensor, Beijing Institute of Nanoenergy and Nanosystems, Chinese Academy of Sciences, Beijing 101400, China; School of Nanoscience and Technology, University of Chinese Academy of Sciences, Beijing 100049, China; School of Materials Science and Engineering, Georgia Institute of Technology, Atlanta, Georgia 30332, United States;* orcid.org/0000-0002-5530-0380; Email: zhong.wang@mse.gatech.edu

Guang Zhu − *CAS Center for Excellence in Nanoscience, Beijing Key Laboratory of Micro-Nano Energy and Sensor, Beijing Institute of Nanoenergy and Nanosystems, Chinese Academy of Sciences, Beijing 101400, China; New Materials Institute, Department of Mechanical, Materials and Manufacturing Engineering, University of Nottingham Ningbo China, Ningbo 315100, China;* orcid.org/0000-0003-2350-0369; Email: zhuguang@binn.cas.cn

Authors

Xin Li − *CAS Center for Excellence in Nanoscience, Beijing Key Laboratory of Micro-Nano Energy and Sensor, Beijing Institute of Nanoenergy and Nanosystems, Chinese Academy of Sciences, Beijing 101400, China; School of Nanoscience and Technology, University of Chinese Academy of Sciences, Beijing 100049, China*

Jinwei Cao − *New Materials Institute, Department of Mechanical, Materials and Manufacturing Engineering, University of Nottingham Ningbo China, Ningbo 315100, China; CAS Key Laboratory of Magnetic Materials and Devices, Ningbo Institute of Materials Technology and Engineering, Chinese Academy of Sciences, Ningbo 315201, China*

Huayang Li − *New Materials Institute, Department of Mechanical, Materials and Manufacturing Engineering, University of Nottingham Ningbo China, Ningbo 315100, China; CAS Key Laboratory of Magnetic Materials and Devices, Ningbo Institute of Materials Technology and Engineering, Chinese Academy of Sciences, Ningbo 315201, China*

Pengtao Yu − *CAS Center for Excellence in Nanoscience, Beijing Key Laboratory of Micro-Nano Energy and Sensor, Beijing Institute of Nanoenergy and Nanosystems, Chinese Academy of Sciences, Beijing 101400, China; School of Nanoscience and Technology, University of Chinese Academy of Sciences, Beijing 100049, China*

Youjun Fan − *CAS Center for Excellence in Nanoscience, Beijing Key Laboratory of Micro-Nano Energy and Sensor, Beijing Institute of Nanoenergy and Nanosystems, Chinese Academy of Sciences, Beijing 101400, China; School of Nanoscience and Technology, University of Chinese Academy of Sciences, Beijing 100049, China*

Yuchuan Xiao − *School of Nanoscience and Technology, University of Chinese Academy of Sciences, Beijing 100049, China; CAS Key Laboratory of Standardization and Measurement for Nanotechnology, CAS Center for Excellence*

in Nanoscience, National Center for Nanoscience and Technology (NCNST), Beijing 100190, China

Yiming Yin − *New Materials Institute, Department of Mechanical, Materials and Manufacturing Engineering, University of Nottingham Ningbo China, Ningbo 315100, China*

Xuejiao Zhao − *CAS Center for Excellence in Nanoscience, Beijing Key Laboratory of Micro-Nano Energy and Sensor, Beijing Institute of Nanoenergy and Nanosystems, Chinese Academy of Sciences, Beijing 101400, China*

Complete contact information is available at: https://pubs.acs.org/10.1021/acsami.1c05572

Author Contributions

[▽]X.L., J.C., and H.L. contributed equally to this work. X.L. and G.Z. conceived and designed the study. X.L. and P.Y. prepared the experimental samples. X.L., P.Y., X.Z., and Y.F. contributed to the data analysis and interpretation. Y.X. carried out the broad outlines of the 3D schematic diagram. X.L. systemically analyzed the experimental results and wrote the manuscripts. J.C., Y.Y., and H.L. participated in the revision of the manuscripts. H.L., Z.W., and G.Z. supervised the research process, and all authors provided feedback.

Notes

The authors declare no competing financial interest.

■ ACKNOWLEDGMENTS

We thank the National Key R & D Project from Ministry of Science and Technology, China (grant no. 2016YFA0202703), Ningbo Municipal 3315 Talent Scheme, Ningbo Scientific and Technological Innovation 2025 Major Project (grant no. 2018B10057), and the Zhejiang Provincial Natural Science Foundation of China (grant no. LR19F010001).

■ REFERENCES

(1) Lim, H. R.; Kim, H. S.; Qazi, R.; Kwon, Y. T.; Jeong, J. W.; Yeo, W. H. Advanced Soft Materials, Sensor Integrations, and Applications of Wearable Flexible Hybrid Electronics in Healthcare, Energy, and Environment. *Adv. Mater.* **2020**, *32*, 1901924.

(2) Zeng, W.; Shu, L.; Li, Q.; Chen, S.; Wang, F.; Tao, X. M. Fiber-Based Wearable Electronics: A Review of Materials, Fabrication, Devices, and Applications. *Adv. Mater.* **2014**, *26*, 5310−5336.

(3) Yang, J. C.; Mun, J.; Kwon, S. Y.; Park, S.; Bao, Z.; Park, S. Electronic Skin: Recent Progress and Future Prospects for Skin-Attachable Devices for Health Monitoring, Robotics, and Prosthetics. *Adv. Mater.* **2019**, *31*, 1904765.

(4) Jung, Y. H.; Park, B.; Kim, J. U.; Kim, T. I. Bioinspired Electronics for Artificial Sensory Systems. *Adv. Mater.* **2019**, *31*, 1803637.

(5) Wang, C.; Li, X.; Hu, H.; Zhang, L.; Huang, Z.; Lin, M.; Zhang, Z.; Yin, Z.; Huang, B.; Gong, H.; Bhaskaran, S.; Gu, Y.; Makihata, M.; Guo, Y.; Lei, Y.; Chen, Y.; Wang, C.; Li, Y.; Zhang, T.; Chen, Z.; et al. Monitoring of The Central Blood Pressure Waveform Via a Conformal Ultrasonic Device. *Nat. Biomed. Eng.* **2018**, *2*, 687−695.

(6) Hwang, G. T.; Byun, M.; Jeong, C. K.; Lee, K. J. Flexible Piezoelectric Thin-Film Energy Harvesters and Nanosensors for Biomedical Applications. *Adv. Healthcare Mater.* **2015**, *4*, 646−658.

(7) Liu, Y.; Pharr, M.; Salvatore, G. A. Lab-on-Skin: A Review of Flexible and Stretchable Electronics for Wearable Health Monitoring. *ACS Nano* **2017**, *11*, 9614−9635.

(8) Pu, X.; Liu, M.; Chen, X.; Sun, J.; Du, C.; Zhang, Y.; Zhai, J.; Hu, W.; Wang, Z. L. Ultrastretchable Transparent Triboelectric Nanogenerator as Electronic Skin for Biomechanical Energy Harvesting and Tactile Sensing. *Sci. Adv.* **2017**, *3*, No. e1700015.

(9) Trung, T. Q.; Lee, N. E. Flexible and Stretchable Physical Sensor Integrated Platforms for Wearable Human-Activity Monitoringand Personal Healthcare. *Adv. Mater.* **2016**, *28*, 4338−4372.

(10) Xie, Z.; Avila, R.; Huang, Y.; Rogers, J. A. Flexible and Stretchable Antennas for Biointegrated Electronics. *Adv. Mater.* **2020**, *32*, 1902767.

(11) Zhu, Z.; Li, R.; Pan, T. J. Imperceptible Epidermal−Iontronic Interface for Wearable Sensing. *Adv. Mater.* **2017**, *30*, 1705121−1705129.

(12) Shin, K.-Y.; Lee, J. S.; Jang, J. Highly Sensitive, Wearable and Wireless Pressure Sensor Using Free-Standing ZnO Nanoneedle/PVDF Hybrid Thin Film for Heart Rate Monitoring. *Nano Energy* **2016**, *22*, 95−104.

(13) Lee, J.; Kwon, H.; Seo, J.; Shin, S.; Koo, J. H.; Pang, C.; Son, S.; Kim, J. H.; Jang, Y. H.; Kim, D. E.; Lee, T. Conductive Fiber-Based Ultrasensitive Textile Pressure Sensor for Wearable Electronics. *Adv. Mater.* **2015**, *27*, 2433−2439.

(14) Ma, L.; Zhou, M.; Wu, R.; Patil, A.; Gong, H.; Zhu, S.; Wang, T.; Zhang, Y.; Shen, S.; Dong, K.; Yang, L.; Wang, J.; Guo, W.; Wang, Z. L. Continuous and Scalable Manufacture of Hybridized Nano-Micro Triboelectric Yarns for Energy Harvesting and Signal Sensing. *ACS Nano* **2020**, *14*, 4716−4726.

(15) Avilés, F.; Oliva-Avilés, A. I.; Cen-Puc, M. Piezoresistivity, Strain, and Damage Self-Sensing of Polymer Composites Filled with Carbon Nanostructures. *Adv. Eng. Mater.* **2018**, *20*, 1701159.

(16) Lee, Y.; Park, J.; Cho, S.; Shin, Y. E.; Lee, H.; Kim, J.; Myoung, J.; Cho, S.; Kang, S.; Baig, C.; Ko, H. Flexible Ferroelectric Sensors with Ultrahigh Pressure Sensitivity and Linear Response over Exceptionally Broad Pressure Range. *ACS Nano* **2018**, *12*, 4045−4054.

(17) Oh, J.; Yang, J. C.; Kim, J. O.; Park, H.; Kwon, S. Y.; Lee, S.; Sim, J. Y.; Oh, H. W.; Kim, J.; Park, S. Pressure Insensitive Strain Sensor with Facile Solution-Based Process for Tactile Sensing Applications. *ACS Nano* **2018**, *12*, 7546−7553.

(18) Liu, M.; Pu, X.; Jiang, C.; Liu, T.; Huang, X.; Chen, L.; Du, C.; Sun, J.; Hu, W.; Wang, Z. L. Large-Area All-Textile Pressure Sensors for Monitoring Human Motion and Physiological Signals. *Adv. Mater.* **2017**, *29*, 1703700.

(19) Gong, S.; Schwalb, W.; Wang, Y.; Chen, Y.; Tang, Y.; Si, J.; Shirinzadeh, B.; Cheng, W. A Wearable and Highly Sensitive Pressure Sensor with Ultrathin Gold Nanowires. *Nat. Commun.* **2014**, *5*, 3132.

(20) Ma, Y.; Liu, N.; Li, L.; Hu, X.; Zou, Z.; Wang, J.; Luo, S.; Gao, Y. A Highly Flexible and Sensitive Piezoresistive Sensor Based on MXene with Greatly Changed Interlayer Distances. *Nat. Commun.* **2017**, *8*, 1207.

(21) Pang, C.; Lee, G. Y.; Kim, T. I.; Kim, S. M.; Kim, H. N.; Ahn, S. H.; Suh, K. Y. A Flexible and Highly Sensitive Strain-Gauge Sensor Using Reversible Interlocking of Nanofibres. *Nat. Mater.* **2012**, *11*, 795−801.

(22) Won, S. M.; Wang, H.; Kim, B. H.; Lee, K.; Jang, H.; Kwon, K.; Han, M.; Crawford, K. E.; Li, H.; Lee, Y.; Yuan, X.; Kim, S. B.; Oh, Y. S.; Jang, W. J.; Lee, J. Y.; Han, S.; Kim, J.; Wang, X.; Xie, Z.; Zhang, Y.; et al. Multimodal Sensing with a Three-Dimensional Piezoresistive Structure. *ACS Nano* **2019**, *13*, 10972−10979.

(23) Wang, Z.; Guan, X.; Huang, H.; Wang, H.; Lin, W.; Peng, Z. Full 3D Printing of Stretchable Piezoresistive Sensor with Hierarchical Porosity and Multimodulus Architecture. *Adv. Funct. Mater.* **2019**, *29*, 1807569.

(24) Lai, Y.-C.; Ye, B.-W.; Lu, C.-F.; Chen, C.-T.; Jao, M.-H.; Su, W.-F.; Hung, W.-Y.; Lin, T.-Y.; Chen, Y.-F. Extraordinarily Sensitive and Low-Voltage Operational Cloth-Based Electronic Skin for Wearable Sensing and Multifunctional Integration Uses: A Tactile-Induced Insulating-to-Conducting Transition. *Adv. Funct. Mater.* **2016**, *26*, 1286−1295.

(25) Yang, Z.; Pang, Y.; Han, X. L.; Yang, Y.; Ling, J.; Jian, M.; Zhang, Y.; Yang, Y.; Ren, T. L. Graphene Textile Strain Sensor with Negative Resistance Variation for Human Motion Detection. *ACS Nano* **2018**, *12*, 9134−9141.

(26) Liu, W.; Liu, N.; Yue, Y.; Rao, J.; Cheng, F.; Su, J.; Liu, Z.; Gao, Y. Piezoresistive Pressure Sensor Based on Synergistical Innerconnect Polyvinyl Alcohol Nanowires/Wrinkled Graphene Film. *Small* **2018**, *14*, 1704149.
(27) Wang, R.; Jiang, N.; Su, J.; Yin, Q.; Zhang, Y.; Liu, Z.; Lin, H.; Moura, F. A.; Yuan, N.; Roth, S.; Rome, R. S.; Ovalle-Robles, R.; Inoue, K.; Yin, S.; Fang, S.; Wang, W.; Ding, J.; Shi, L.; Baughman, R. H.; Liu, Z. A Bi-Sheath Fiber Sensor for Giant Tensile and Torsional Displacements. *Adv. Funct. Mater.* **2017**, *27*, 1702134.
(28) Park, S.; Kim, H.; Vosgueritchian, M.; Cheon, S.; Kim, H.; Koo, J. H.; Kim, T. R.; Lee, S.; Schwartz, G.; Chang, H.; Bao, Z. Stretchable Energy-Harvesting Tactile Electronic Skin Capable of Differentiating Multiple Mechanical Stimuli Modes. *Adv. Mater.* **2014**, *26*, 7324−7332.
(29) Wang, H.; Song, Y.; Guo, H.; Wan, J.; Miao, L.; Xu, C.; Ren, Z.; Chen, X.; Zhang, H. A Three-Electrode Multi-Module Sensor for Accurate Bodily-Kinesthetic Monitoring. *Nano Energy* **2020**, *68*, 104316.
(30) Choi, S.; Yoon, K.; Lee, S.; Lee, H. J.; Lee, J.; Kim, D. W.; Kim, M. S.; Lee, T.; Pang, C. Conductive Hierarchical Hairy Fibers for Highly Sensitive, Stretchable, and Water-Resistant Multimodal Gesture-Distinguishable Sensor, VR Applications. *Adv. Funct. Mater.* **2019**, *29*, 1905808.
(31) Sang, Z.; Ke, K.; Manas-Zloczower, I. Design Strategy for Porous Composites Aimed at Pressure Sensor Application. *Small* **2019**, *15*, 1903487.
(32) Park, J.; Lee, Y.; Hong, J.; Lee, Y.; Ha, M.; Jung, Y.; Lim, H.; Kim, S. Y.; Ko, H. Tactile-Direction-Sensitive and Stretchable Electronic Skins Based on Human-Skin-Inspired Interlocked Microstructures. *ACS Nano* **2014**, *8*, 12020.
(33) Ding, X.; Zhong, W.; Jiang, H.; Li, M.; Chen, Y.; Lu, Y.; Ma, J.; Yadav, A.; Yang, L.; Wang, D. Highly Accurate Wearable Piezoresistive Sensors without Tension Disturbance Based on Weaved Conductive Yarn. *ACS Appl. Mater. Interfaces* **2020**, *12*, 35638.
(34) Wang, Q.; Yan, J.; Fan, Z. Carbon Materials for High Volumetric Performance Supercapacitors: Design, Progress, Challenges and Opportunities. *Energy Environ. Sci.* **2016**, *9*, 729−762.
(35) Yao, H. B.; Ge, J.; Wang, C. F.; Wang, X.; Hu, W.; Zheng, Z. J.; Ni, Y.; Yu, S. H. A Flexible and Highly Pressure-Sensitive Graphene-Polyurethane Sponge Based on Fractured Microstructure Design. *Adv. Mater.* **2013**, *25*, 6692−6698.
(36) Fan, Y. J.; Meng, X. S.; Li, H. Y.; Kuang, S. Y.; Zhang, L.; Wu, Y.; Wang, Z. L.; Zhu, G. Stretchable Porous Carbon Nanotube-Elastomer Hybrid Nanocomposite for Harvesting Mechanical Energy. *Adv. Mater.* **2017**, *29*, 1603115.
(37) Qiu, L.; Liu, J. Z.; Chang, S. L. Y.; Wu, Y.; Li, D. Biomimetic Superelastic Graphene-Based Cellular Monoliths. *Nat. Commun.* **2012**, *3*, 1241.
(38) Chen, X.; Liu, H.; Zheng, Y.; Zhai, Y.; Liu, X.; Liu, C.; Mi, L.; Guo, Z.; Shen, C. Highly Compressible and Robust Polyimide/Carbon Nanotube Composite Aerogel for High-Performance Wearable Pressure Sensor. *ACS Appl. Mater. Interfaces* **2019**, *11*, 42594−42606.
(39) Liu, L.; Li, H. Y.; Fan, Y. J.; Chen, Y. H.; Kuang, S. Y.; Li, Z. B.; Wang, Z. L.; Zhu, G. Nanofiber-Reinforced Silver Nanowires Network as a Robust, Ultrathin, and Conformable Epidermal Electrode for Ambulatory Monitoring of Physiological Signals. *Small* **2019**, *15*, 1900755.
(40) Li, X.; Fan, Y. J.; Li, H. Y.; Cao, J. W.; Xiao, Y. C.; Wang, Y.; Liang, F.; Wang, H. L.; Jiang, Y.; Wang, Z. L.; Zhu, G. Ultracomfortable Hierarchical Nanonetwork for Highly Sensitive Pressure Sensor. *ACS Nano* **2020**, *14*, 9605−9612.
(41) Fan, Y. J.; Yu, P. T.; Liang, F.; Li, X.; Li, H. Y.; Liu, L.; Cao, J. W.; Zhao, X. J.; Wang, Z. L.; Zhu, G. Highly Conductive, Stretchable, and Breathable Epidermal Electrode Based on Hierarchically Interactive Nano-Network. *Nanoscale* **2020**, *12*, 16053−16062.

https://doi.org/10.1021/acsami.1c05572
ACS Appl. Mater. Interfaces XXXX, XXX, XXX−XXX